

## Supporting information for Ultralow Thermal Conductivity and High Thermoelectric Figure of Merit in Mixed Valence $\text{In}_5\text{X}_5\text{Br}$ (X = S, and Se) Compounds

Tribhuvan Pandey, Arun Nissimagoudar, Avanish Mishra and Abhishek K. Singh

Materials Research Centre, Indian Institute of Science, Bangalore 560012, India

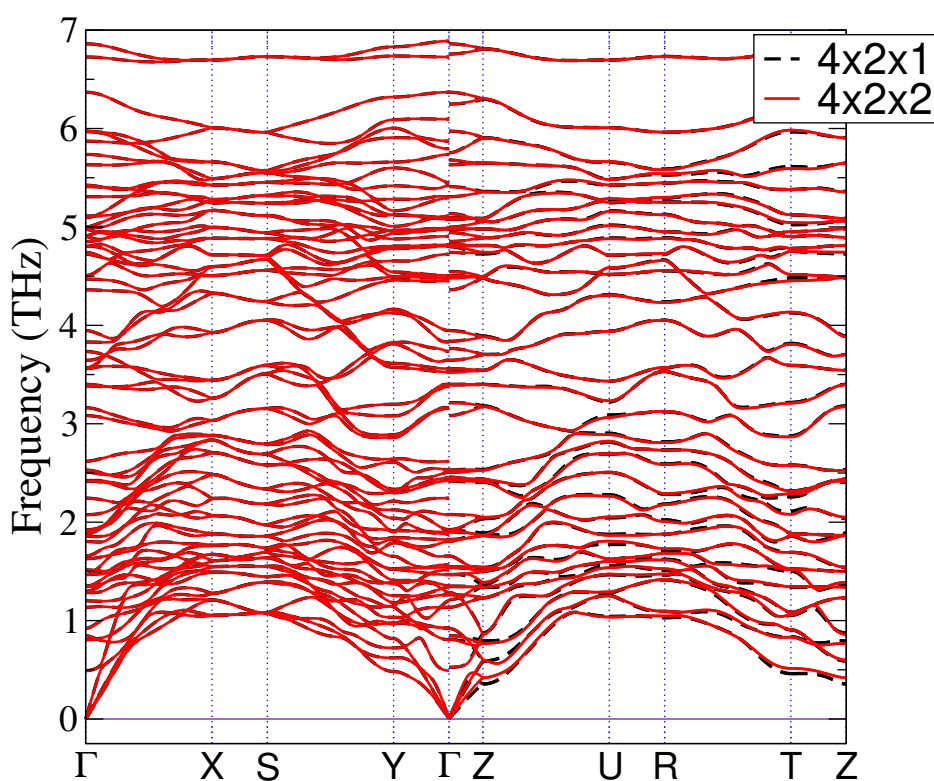


FIG. S1. Convergence of phonon dispersion with respect to supercell size for  $\text{In}_5\text{Se}_5\text{Br}$ . The dashed black lines corresponds to calculation performed with  $4 \times 2 \times 1$  supercell, and red solid lines corresponds to calculation with  $4 \times 2 \times 2$  supercell. As can be seen the phonon dispersion is well converged with respect to supercell size and  $4 \times 2 \times 2$  supercell was used in all the calculations presented in the main manuscript.

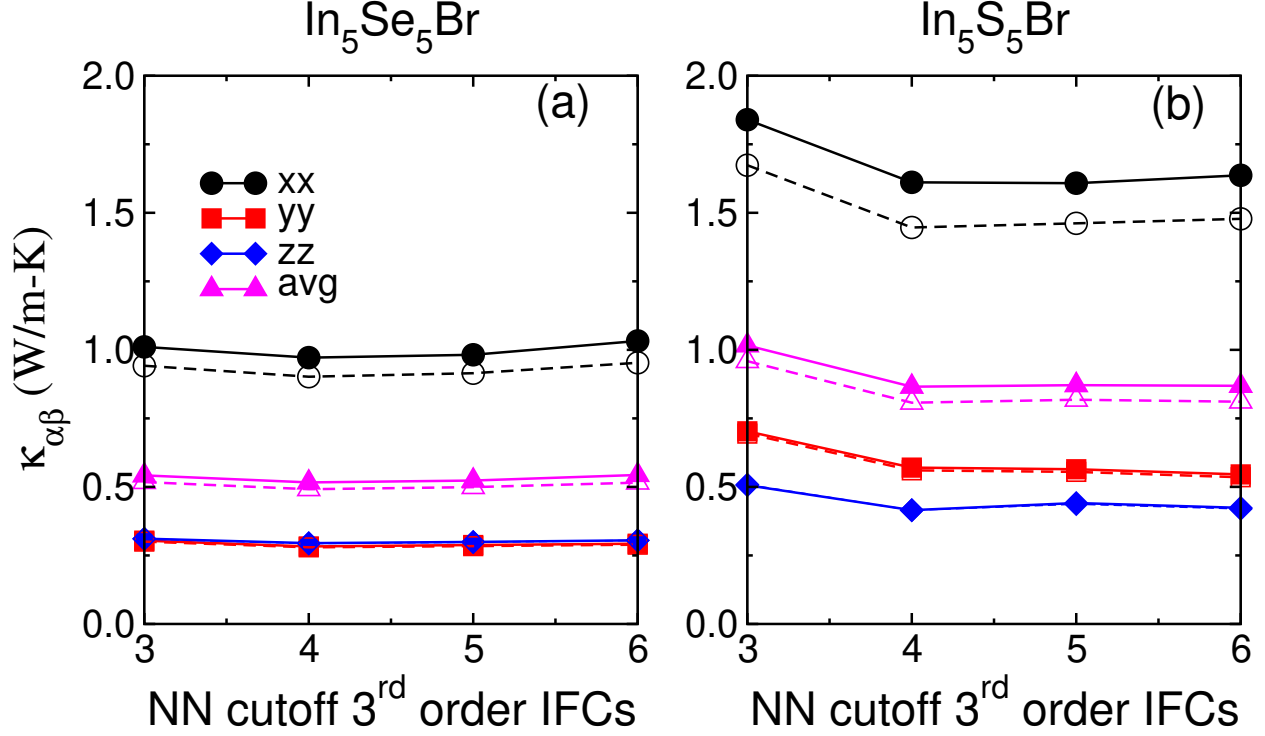


FIG. S2. Convergence of lattice thermal conductivity with respect to 3rd order inter atomic force constants cutoff for (a)  $\text{In}_5\text{Se}_5\text{Br}$  and (b)  $\text{In}_5\text{S}_5\text{Br}$ . The solid and dashed line present the lattice thermal conductivity by full solution of Boltzmann transport equation, and within relaxation time approximation, respectively. The calculation presented in the main manuscript are done with IFCs with cutoff upto 6<sup>th</sup> nearest neighbor. Both harmonic and anharmonic force constants employed in the convergence test are computed on  $4 \times 2 \times 2$  supercell.

TABLE S1. The GGA optimized lattice parameters along the bandgaps calculated under GGA+SOC, and TB-mBJ+SOC. The values in brackets are the experimental lattice parameters from reference [3].

system	lattice parameters ( $\text{\AA}$ )			Bandgap (eV)	
	a	b	c	GGA+SOC	TB-mBJ+SOC
$\text{In}_5\text{S}_5\text{Br}$	4.00 (3.92)	9.22 (9.05)	15.30 (14.81)	1.08	1.556
$\text{In}_5\text{Se}_5\text{Br}$	4.17 (4.10)	9.47 (9.33)	15.82 (15.25)	0.721	1.087

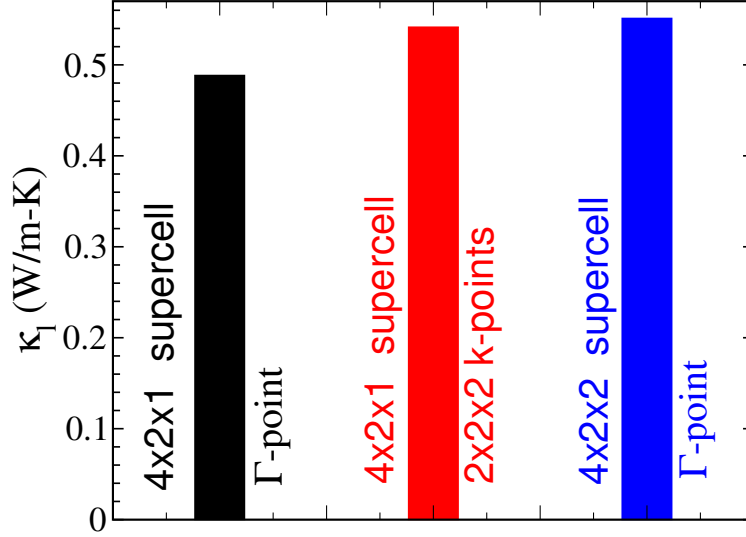


FIG. S3. Convergence of room temperature lattice thermal conductivity with respect to supercell size, and k-points used in the calculation of anharmonic inter-atomic force constants (IFCs). These calculations use anharmonic IFCs where interactions are truncated at 4<sup>th</sup> nearest neighbors. For all three cases the harmonic IFCs are computed on 4×2×2 supercell, and integration grid of 25×12×8 was used for the solving the Boltzmann transport equation. The k-point used during computation of anharmonic IFCs has nominal effect on the final  $\kappa_l$ . Between  $\Gamma$ -points only (black bar), and 2×2×2 k-point (red bar) calculations the variation in  $\kappa_l$  is less than 3 %.

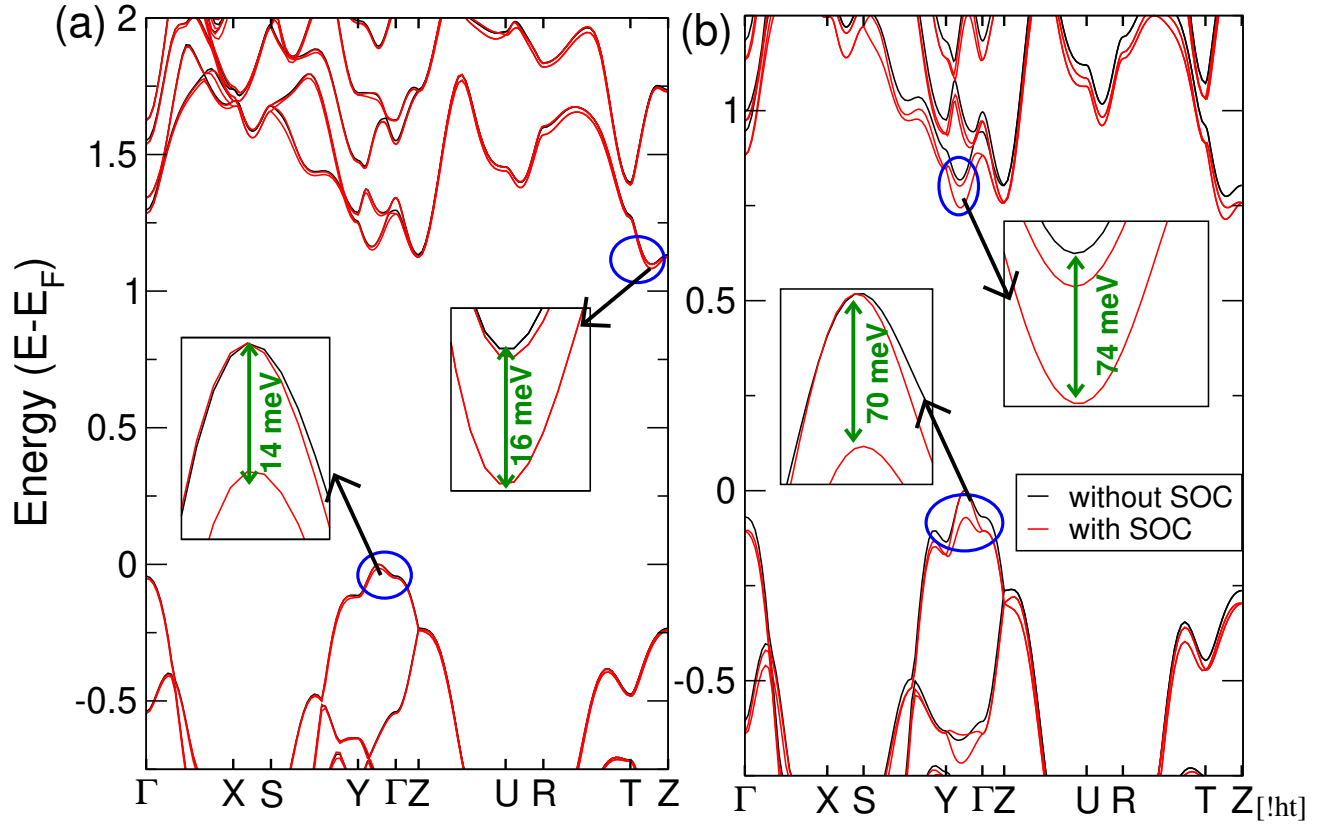


FIG. S4. Effect of spin orbit coupling on electronic structure of (a)  $\text{In}_5\text{S}_5\text{Br}$ , and (b)  $\text{In}_5\text{Se}_5\text{Br}$ , as calculated with in GGA (black lines), and GGA+SOC calculations (red lines). The largest splitting of both valence and conduction bands due to spin orbit coupling in shown in the inset in each plot. For  $\text{In}_5\text{S}_5\text{Br}$  a small spin orbit splitting of 14 meV, and 16 meV was observed at valence band maxima (between Y- $\Gamma$  directions), and at conduction band maxima (between T-Z directions). For  $\text{In}_5\text{Se}_5\text{Br}$  a larger spin orbit splitting of  $\sim 70$  meV was observed.

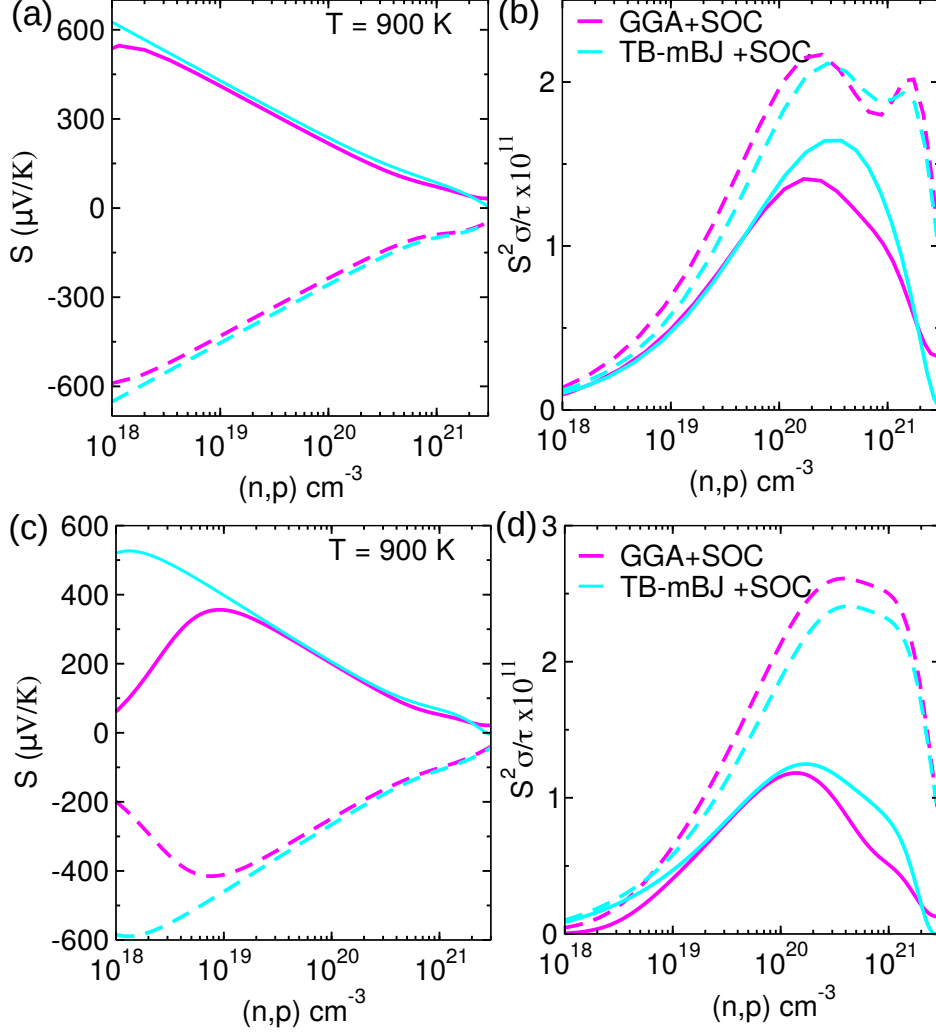


FIG. S5. Comparison of thermopower and power factor at 900 K with the GGA+SOC bandgap (magenta lines), and TB-mBJ+SOC bandgap (cyan lines) (listed in Table S1) as a function of carrier concentration. (a), and (b) present thermopower and power factor for  $\text{In}_5\text{S}_5\text{Br}$ ; (c), and (d) give the same information for  $\text{In}_5\text{Se}_5\text{Br}$ . The solid and dashed lines denote results for  $p$ -type and  $n$ -type doping, respectively. With the larger TB-mBJ bandgap the thermopower is slightly higher for both systems in the relevant doping ( $75 \times 10^{19} \text{ cm}^{-3} - 3 \times 10^{20} \text{ cm}^{-3}$ ) and temperature ranges. The slight decrease in  $n$ -type power factor with larger bandgaps is due to lower electrical conductivity. Whereas under  $p$ -type doping powerfactor with TB-mBJ bandgaps are bit larger. Nonetheless, both the methods give comparable power factor.

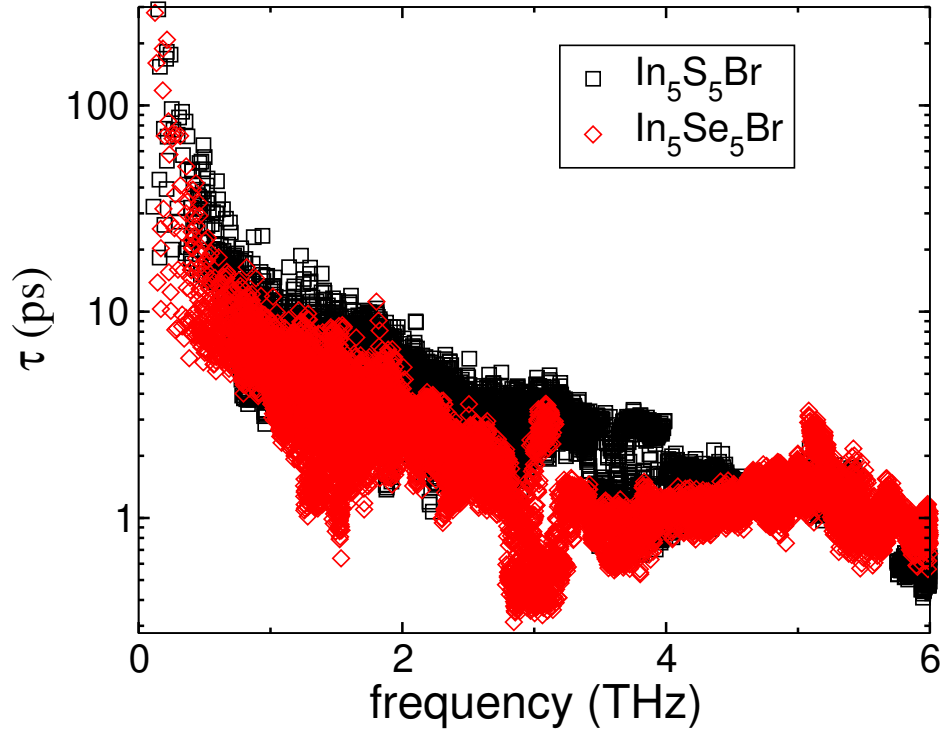


FIG. S6. Variation of room temperature phonon lifetimes ( $\tau$ ) as function of phonon frequencies for  $\text{In}_5\text{S}_5\text{Br}$  (open black squares), and  $\text{In}_5\text{Se}_5\text{Br}$  (open red diamonds). As can be seen between the frequency window 0-4 THz  $\tau$  of  $\text{In}_5\text{Se}_5\text{Br}$  is an order of magnitude smaller than that of  $\text{In}_5\text{S}_5\text{Br}$ . This is main reason for relatively low lattice thermal conductivity of  $\text{In}_5\text{Se}_5\text{Br}$ .

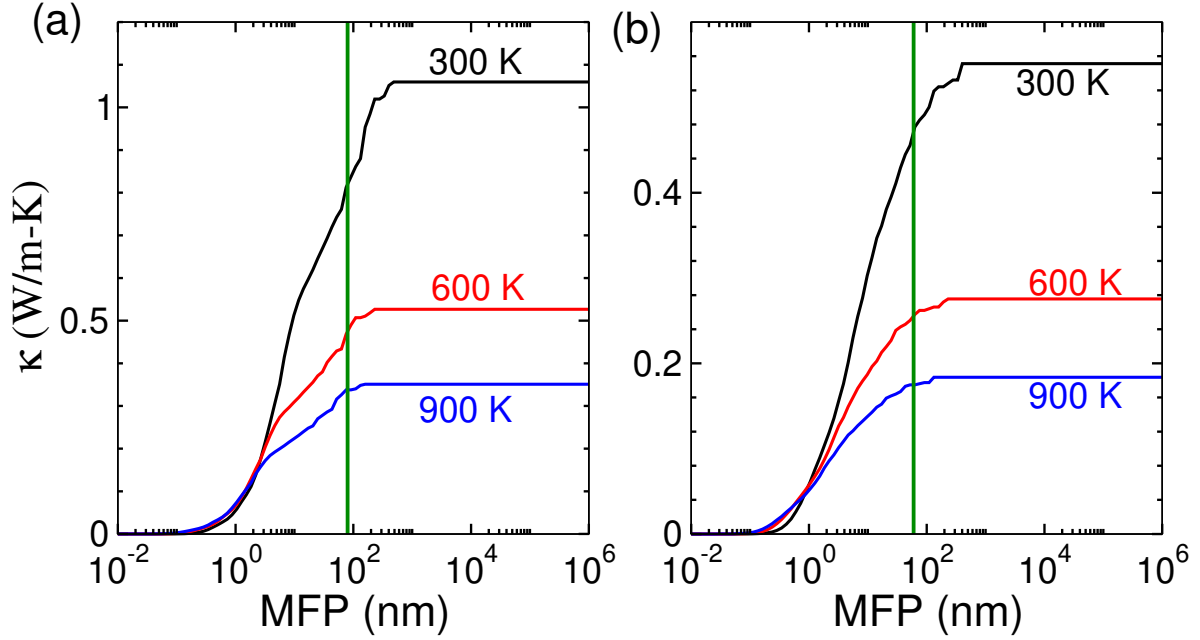


FIG. S7. Cumulative 300 K, 600 K, and 900 K lattice thermal conductivity as a function of phonon mean free path for (a) In<sub>5</sub>S<sub>5</sub>Br, and (b) In<sub>5</sub>Se<sub>5</sub>Br. For both the compounds majority of the heat is carried by phonons with mean free path < 80 nm (shown by green vertical line). For example at 300 K for In<sub>5</sub>S<sub>5</sub>Br the 80 % of heat is carried by phonons with mean free path less than 80 nm. Similarly for In<sub>5</sub>Se<sub>5</sub>Br at room temperature majority of heat is carried by phonon with mean free path less than 60 nm. This indicates that nanostructuring with grains smaller 60-80 nm, could help to further reduce the lattice thermal conductivity of these materials.

### A. Electron relaxation time

Another essential requirement for the calculation of transport properties is the relaxation time,  $\tau(E)$  arising from different scattering mechanisms. The electrons may undergo collisions with acoustic phonons, optical phonons, and impurities present in the system. Different scattering mechanisms may dominate at different temperatures [1]. In the temperature range of interest ( $100 < T < 1200$  K), the scattering processes limiting electron transport are the scattering of electrons with acoustic and optical phonons. While the scattering of electrons by acoustical phonons dominates at low temperatures, the scattering from optical phonons plays an important role at higher temperatures. The electron relaxation rates due to scattering by acoustical phonons can be described by [1, 2],

$$(\tau_{AP}(E))^{-1} = \frac{(2m^*)^{3/2} D_{ac}^2 k_B T}{2\pi v_{LA}^2 \hbar^4 \rho} E^{1/2} \quad (S1)$$

where  $m^*$ ,  $v_{LA}$ ,  $\rho$ ,  $T$ ,  $D_{ac}$ ,  $\hbar$ , and  $k_B$  are effective mass of carriers, longitudinal sound velocity, mass density, temperature, deformation potential, Planck's constants and Boltzmann constant, respectively. Similarly, due to scattering by optical phonons the relaxation rate can be given by [1, 2],

$$\begin{aligned} (\tau_{OP}(E))^{-1} = & \frac{e^2 \omega_{LO}}{4\sqrt{2}\varepsilon_0 \hbar} \left( \frac{1}{\kappa_\infty} - \frac{1}{\kappa_0} \right) \frac{\sqrt{m^*}}{\sqrt{E}} \left[ (n_q + 1) \right. \\ & \left. \left\{ \sqrt{1 - \frac{\hbar\omega_{LO}}{E}} + \frac{\hbar\omega_{LO}}{E} \sinh^{-1} \left( \frac{E}{\hbar\omega_{LO}} - 1 \right)^{1/2} \right\} \right. \\ & \left. + (n_q) \left\{ \sqrt{1 + \frac{\hbar\omega_{LO}}{E}} - \frac{\hbar\omega_{LO}}{E} \sinh^{-1} \left( \frac{E}{\hbar\omega_{LO}} \right)^{1/2} \right\} \right] \quad (S2) \end{aligned}$$

Here  $e$ ,  $n_q$ ,  $\omega_{LO}$ ,  $\kappa_\infty$ ,  $\kappa_0$ , and  $\varepsilon_0$  are the electronic charge, Fermi-Dirac distribution function, longitudinal optical phonon frequency, relative permittivity at high frequency, static dielectric constant, and permittivity of free space, respectively.

The numerical calculations of relaxation time are performed using the physical quantities given in Table S2. Figure S8 (a) shows the variation of electron relaxation time due to the scattering by acoustic, and polar optical phonons for  $\text{In}_5\text{S}_5\text{Br}$ . The overall contribution to relaxation time is calculated by Mattheissen's rule. In these calculations the carrier concentration is fixed at  $n = 3 \times 10^{19} \text{ cm}^{-3}$ . With the increase in temperature, more phonons modes get excited leading to the enhancement in the scattering of electrons, thereby reducing the relaxation time. The magnitude of relaxation time varies from  $7 \times 10^{-13}$  s to  $9 \times 10^{-14}$  s. The temperature variation of total relaxation time for  $\text{In}_5\text{S}_5\text{Br}$  at three different carrier concentration is shown in Figure S8 (b). As expected

TABLE S2. The physical parameters used for the calculation of electron relaxation time for  $\text{In}_5\text{S}_5\text{Br}$  and  $\text{In}_5\text{Se}_5\text{Br}$ .

Parameter	System	
	$\text{In}_5\text{S}_5\text{Br}$	$\text{In}_5\text{Se}_5\text{Br}$
Relative permittivity at high frequency ( $\kappa_\infty$ )	7.95	10.6
Static dielectric constant ( $\kappa_0$ )	8.23	11.75
Number of atoms per unit cell ( $V$ )	22	22
Mass density ( $\rho$ ) in $\text{kg}/\text{m}^3$	5143	5970
Deformation potential constant ( $D_{ac}$ ) in eV	3.51	2.97
Effective mass of electron ( $m_e$ )	$0.57m_e$	$0.4m_e$
Longitudinal sound velocity ( $v_{LA}$ ) in m/s	2709	2559

with the increase in carrier concentration the relaxation time increases due to the enhancement of electron-polar optical phonon scattering. The computed relaxation time for  $\text{In}_5\text{Se}_5\text{Br}$  is shown in Figure S8 (c) and (d). These relaxation rates are used to calculate the  $ZT$  (discussed in the manuscript).

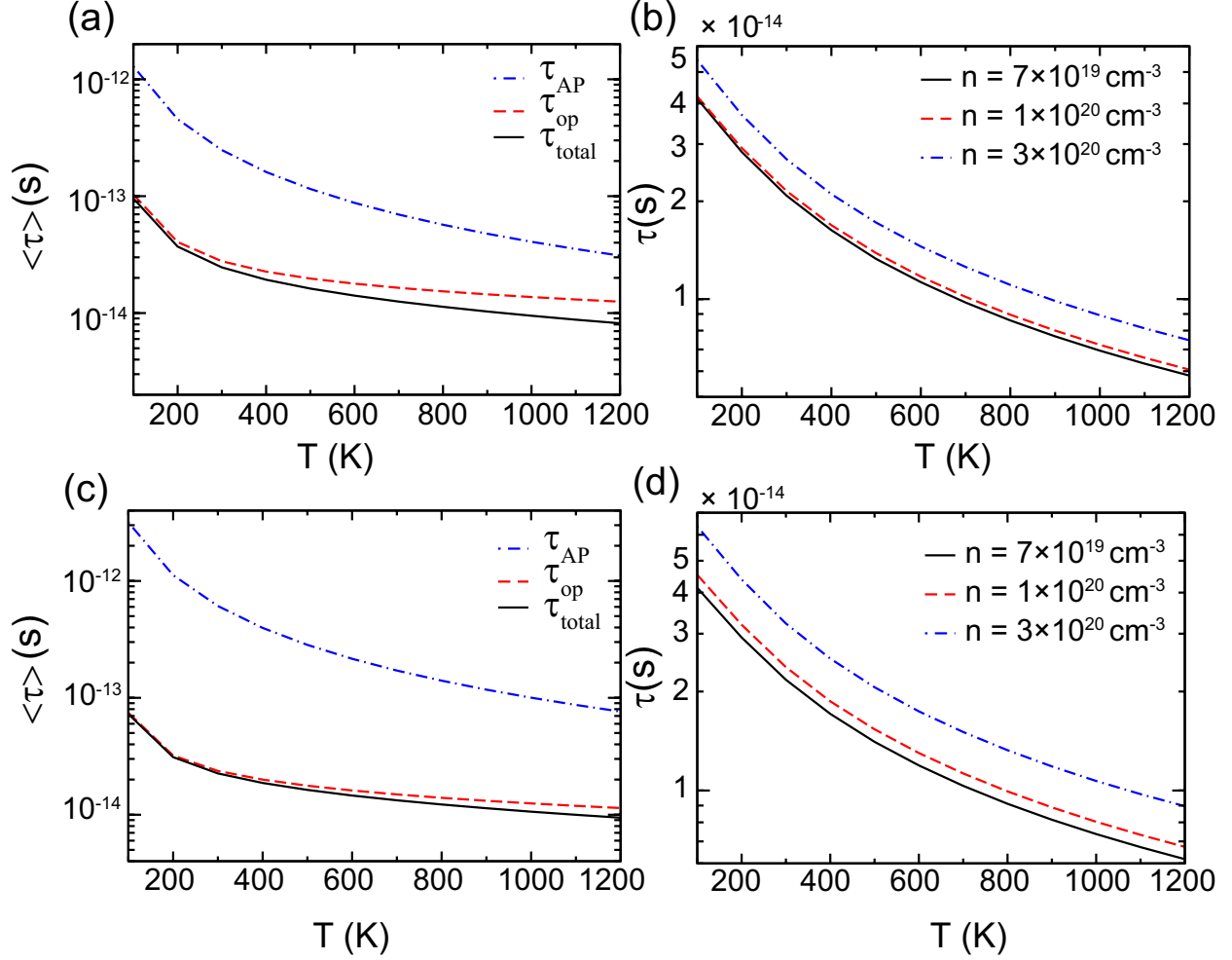


FIG. S8. (a) Temperature variation of relaxation times in  $\text{In}_5\text{S}_5\text{Br}$  from electron-acoustic scattering ( $\tau_{AP}$ ), electron-polar optical phonon scattering ( $\tau_{OP}$ ), along with total relaxation time ( $\tau_{total}$ ) calculated using the Matthiessen's rule. These calculations are done at a fixed carrier concentration of  $3 \times 10^{20} \text{cm}^{-3}$ . (b) Overall relaxation time for three different carrier concentrations. (c) and (d) present same information for  $\text{In}_5\text{Se}_5\text{Br}$ .

- 
- [1] B. R. Nag, *Electron Transport in Compound Semiconductors*, Vol. 11 (Springer Science & Business Media, 2012).
- [2] C. Hamaguchi, *Basic Semiconductor Physics* (Springer Science & Business Media, 2009).
- [3] H.-J. Deiseroth, C. Reiner, K. Xhaxhiu, M. Schlosser, and L. Kienle, *Z. Anorg. Allg. Chem.* **630**, 2319 (2004).